Influence of Surface Topography on Heat Transfer in Shear-Driven Liquid Films

Mete Budakli[1], Tatiana Gambaryan-Roisman[1, 2] and Peter Stephan[1, 2, 3]

[1]Institute of Technical Thermodynamics, Technische Universität Darmstadt, Petersenstraße 32, 64287 Darmstadt, Germany

[2]Center of Smart Interfaces, Technische Universität Darmstadt, Petersenstraße 32, 64287 Darmstadt, Germany

Abstract. Thin gas-driven liquid films find numerous industrial applications. They are used for fuel preparation in airblast atomizers of modern gas turbines. Strong shear forces at the gas-liquid interface destabilize the liquid-gas interface and lead to development of interfacial waves. In this study, the heat transfer in liquid films driven by turbulent gas flow is investigated experimentally over a wide range of parameters. A liquid film is formed on vertical heated unstructured and micro-structured tubes. The Reynolds number of the gas flow is varied between 10^4 and 10^5, and the Reynolds number of the liquid film flow is varied between 80 and 800. Wall heat fluxes up to 30 W/cm² are applied. The heat transfer coefficient strongly depends on the gas and liquid Reynolds numbers. Using the micro-structured tube leads to a heat transfer enhancement of up to 80 %.

1. Introduction

The recent development of modern gas turbines is driven by the challenge to reduce the NO_x emissions. This can be achieved using the Lean Pre-mixing Pre-vaporizing (LPP) concept of combustion chambers [1]. In LPP systems, the liquid fuel impinges onto a prefilmer and forms a thin film over the prefilmer wall (Figure 1, inset a). The film is accelerated by strong interfacial shear forces caused by the co-current hot air flow. The high shear stresses destabilize the liquid-gas interface and lead to development of waves and to entrainment of droplets (Figure 1, insets b and c). The thin film partly evaporates and mixes with the hot gas flow [2]. The atomization/breakup of the liquid film and fuel-air mixing process depend on the hydrodynamics of the wavy film, which thus influences the overall fuel preparation process [3, 4].

Gas flow-driven liquid films are also used in devices for cooling of electronic components [5]. It has been found that for typical process parameters encountered in such applications the gas-driven heated films are more stable against the rupture than the gravity-driven films [6].

The film dynamics and heat and mass transport can be noticeably affected by using micro-structured walls [7-10]. Micro-grooves directed along the main flow direction promote the rivulet flow regime characterized by the presence of contact lines. The liquid evaporation rate in the vicinity of contact lines is extremely high [11], which leads to a significant intensification of evaporation heat transfer on micro-grooved walls [8]. The longitudinal grooves are also known to stabilize the film flow and suppress the wave growth [8, 10]. The micro-grooves oriented perpendicularly to the liquid flow

[3] Corresponding author, e-mail: pstephan@ttd.tu-darmstadt.de

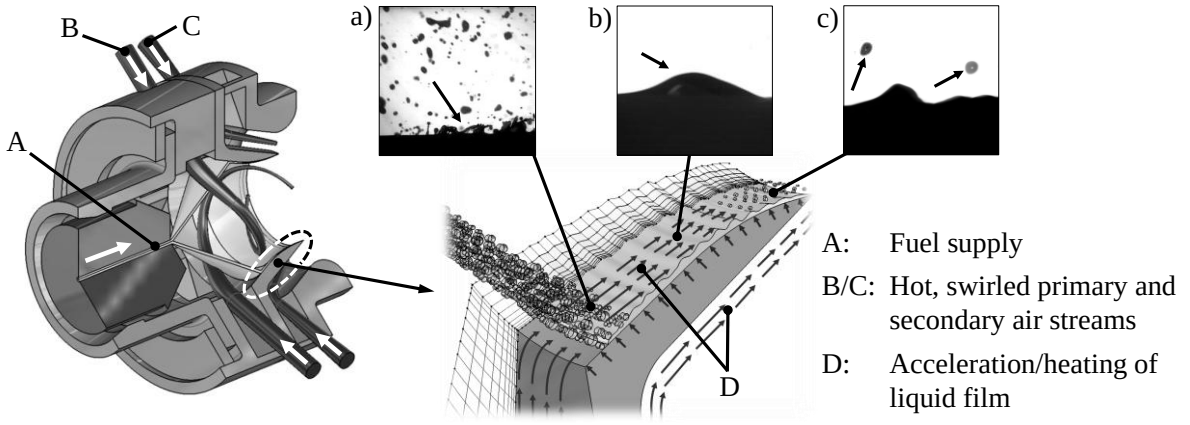

Figure 1. Left: CAD-Model of an LPP-Airblast-Atomizer. Detailed view of near-wall phenomena: a) fuel spray impact and film formation, b) wavy film flow, c) droplet entrainment.

direction lead to heat transfer intensification due to formation of vortices and hence to the intensification of the mixing of liquid [9]. Although a significant progress has been achieved recently in understanding the complex mechanisms of heat transport in wavy shear-driven films on micro-structured walls, a complete understanding of these mechanisms has not yet been achieved, especially for the walls with complex three-dimensional topography.

The objective of the present work is to study the heat transfer in shear-driven films flowing on micro-structured surfaces comprised of micro-pyramid. This topography may combine the advantages of longitudinal microgrooves by promoting the flow patterns with a large cumulative length of contact lines and the advantages of the micro-grooves oriented normal to the main flow direction by promoting the formation of vortices. Using the infrared thermography, the flow patterns in liquid films flowing along a micro-structured tube at different experimental conditions are qualitatively visualized.

2. Experimental setup and measurement techniques

The setup for investigation of hydrodynamics and heat transfer in shear-driven liquid films is schematically shown in Figure 2. The test section consists of an experimental channel surrounding a copper tube (which can be structured or unstructured) with an outer diameter of 19 mm. The details of the test section are shown in Figure 3. The channel has two quartz and one calcium fluoride windows to provide optical access for infrared thermography. The experimental setup shown in Figure 2 operates with a gas (air) and a liquid (deionized water) flow loops. The gas enters the experimental channel, passes a filter and flows concurrently with the liquid film flow (Figure 3). The pressure of the gas has been kept constant at 3 bar using a pressure expansion valve. The inlet temperature of the gas is controlled using an electrical gas heater (10). In the present study the inlet temperature of the gas has been kept constant at 20°C. The mass flow rate of the gas stream is controlled using pressure expansion valve and a thermal mass flow meter (8). The accuracy of the mass flow meter is ± 1.5 % of measurement range.

The liquid is fed to the test channel using a frequency adjusted variable-speed gear pump. The liquid mass flow rate is measured using a Coriolis mass flow meter (3) with an accuracy of ± 0.15 % of reading. The liquid inlet temperature is controlled using a plate heat exchanger (4) together with a high performance thermostat (5). The liquid inlet temperature has been fixed at 25°C. Using a film distributor, the liquid film with an initial thickness of 425 ± 20 μm is annularly spread on the surface of a vertically aligned tube (Figure 3a). This tube has been uniformly heated over the length of l_W = 90 mm by a heating cartridge assembled inside it.

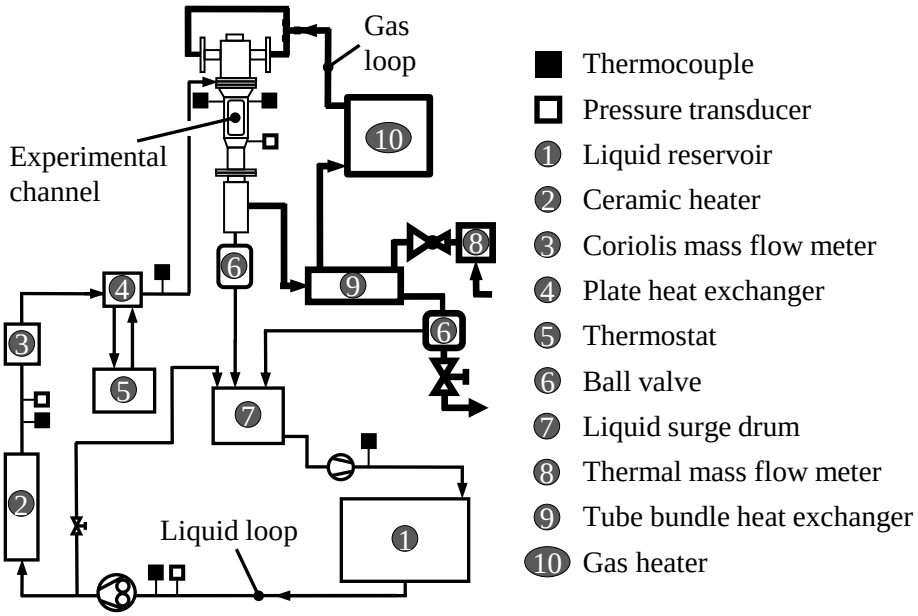

Figure 2. Flow chart of experimental setup for investigation of shear-driven film flows.

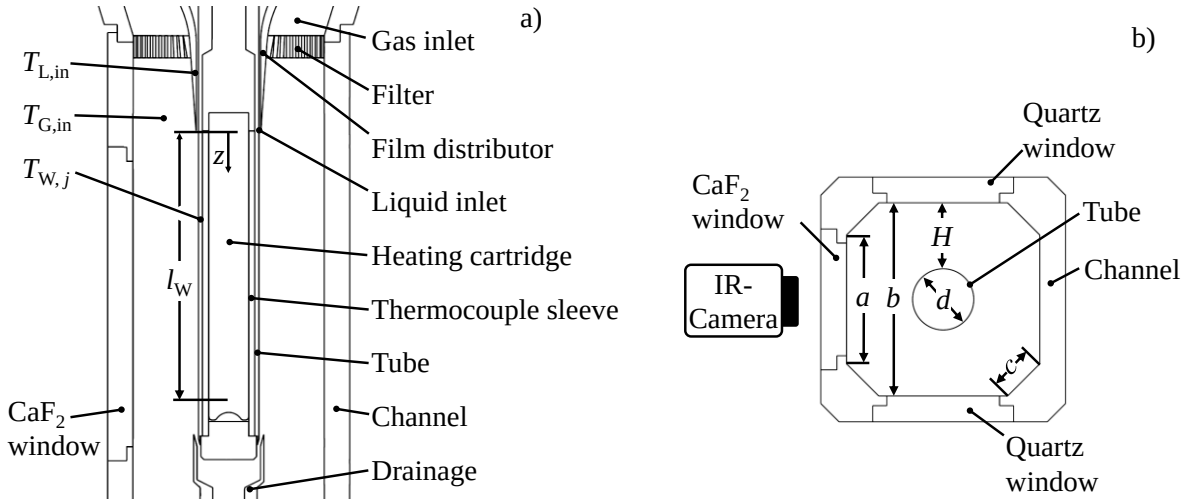

Figure 3. a) Experimental channel in longitudinal cut, b) Cross section at z = 25 mm.

The Reynolds numbers of liquid and gas are calculated using the following relations:

$$Re_{\mathrm{L}} = \frac{M_{\mathrm{L}}}{U_{\mathrm{L}}\mu_{\mathrm{L}}} \quad \text{with} \quad U_{\mathrm{L}} = \pi d \tag{1}$$

$$Re_{\mathrm{G}} = \frac{w_{\mathrm{G}} d_{\mathrm{h}}}{\nu_{\mathrm{G}}} = \frac{1}{\nu_{\mathrm{G}}} \frac{M_{\mathrm{G}}}{A_{\mathrm{G}}\rho_{\mathrm{G}}} \cdot \frac{4A_{\mathrm{G}}}{U_{\mathrm{G}}} = \frac{4M_{\mathrm{G}}}{U_{\mathrm{G}}\mu_{\mathrm{G}}} \quad \text{with} \quad U_{\mathrm{L}} = \pi d + 4\ a + c \tag{2}$$

where M_{L} and M_{G} are the mass flow rates of liquid and gas, respectively, U_{L} is the circumference of the tube, U_{G} is the wetted perimeter of the channel, and μ_{L} and μ_{G} are the dynamic viscosities of the liquid and gas. In this study, the liquid and gas Reynolds numbers were varied between 80-800 and 10^4-10^5, respectively.

The constant wall heat flux applied in the experiment was set to 30 W/cm² and is determined as

$$q_W = \frac{VI}{d\pi l_W}, \tag{3}$$

where V is the voltage and I the input current set at the power supply. The heat losses are not taken into account. The wall heat flux has been determined with a relative error of about ± 0.9 %.
In a sleeve implemented between the heating cartridge and the tube, eight thermocouples are soldered in grooves to measure the wall temperature distribution $T_{W,j}$ in axial direction 1.5 mm below the liquid-wall interface. The liquid and gas inlet temperatures are measured with thermocouples through the film distributor and at the inlet of the experimental channel. The uncertainty in temperature measurements has been estimated to be ± 0.3 K.
The film flow patterns, the break-up and rewetting phenomena have been observed using the infrared (IR) thermography. A high-speed mid-wave IR camera with the array size of 224 × 224 pixels and an image resolution of 14.8 × 14.8 mm² has been used. The images have been taken at an axial distance z = 40 mm from the liquid inlet.
The experiments have been performed with an unstructured tube and with a micro-structured tube. The average roughness of the unstructured tube surface has been measured to be 4 µm. The topography of the micro-structured tube is presented in Figure 4. The micro-structured surface is comprised of pyramids with a height of h_Δ = 500 µm ± 40 µm and a flank angle of $\beta\Delta \sim 120° \pm 5°$.

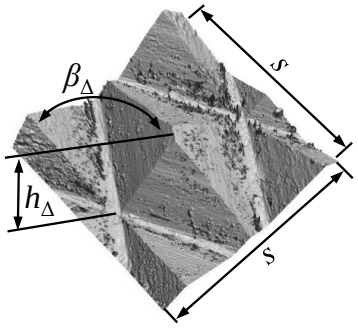

Figure 4. Confocal-microscope image of the micro-structured surface (s = 1600 µm).

3. Results and discussion

3.1. Heat transfer
The local Nusselt numbers Nu have been determined for the axial positions starting from z = 30 mm to z = 65 mm using the relation:

$$Nu = q_W l_W \lambda_L \left(T_{W,j} - T_{L,in}\right)^{-1}, \tag{4}$$

where λ_L (0.6072 W/(m·K)) corresponds to the thermal conductivity of the liquid used in the experiments and l_W is the heated length of the tube. The mean Nusselt numbers Nu_m have been calculated with

$$Nu_m = q_W l_W \lambda_L \left(\frac{1}{n}\sum_{j=1}^{n} T_{W,j} - T_{L,in}\right)^{-1}. \tag{5}$$

The local and mean Nusselt numbers have been determined with a relative error of ± 2.5 %. The distribution of the local heat Nusselt number along the axial direction is presented in Figures 5 and 6. For all combinations of experimental parameters the local Nusselt number decreases along the flow direction. This effect can be explained by the increase of the wall temperature along the axial direction caused by the constant heat flux heating. The decrease of the local Nusselt number is much stronger for the micro-structured tube compared to the unstructured tube. One of the explanations of this strong decrease of local Nusselt number can be a possible deceleration of the film flow along the flow direction caused by large area of the solid-liquid interface for a micro-structured wall and higher wall shear forces compared to unstructured wall. The effect of the gas flow rate on Nusselt number

distribution is demonstrated in Figure 5. For the unstructured tube a ten-fold increase in Re_G results in a doubling of the local Nusselt numbers and to a minor increase in the rate of its decrease with z. This heat transfer intensification is caused by the higher interfacial shear stress at a higher gas Reynolds number. The liquid film velocity increases with increasing the shear stress, which leads to the intensification of convective heat transfer. The local Nusselt numbers at the micro-structured surface for $Re_G = 10^4$ exceed the Nusselt numbers at the unstructured surface (Figure 5b). This effect can be explained by possible formation of vortices in the liquid film which promote the liquid mixing inside the liquid film and thereby intensify the heat transfer. The formation of vortices in a liquid film on a micro-structured surface can be caused by the presence of obstacles along the flow direction [12].

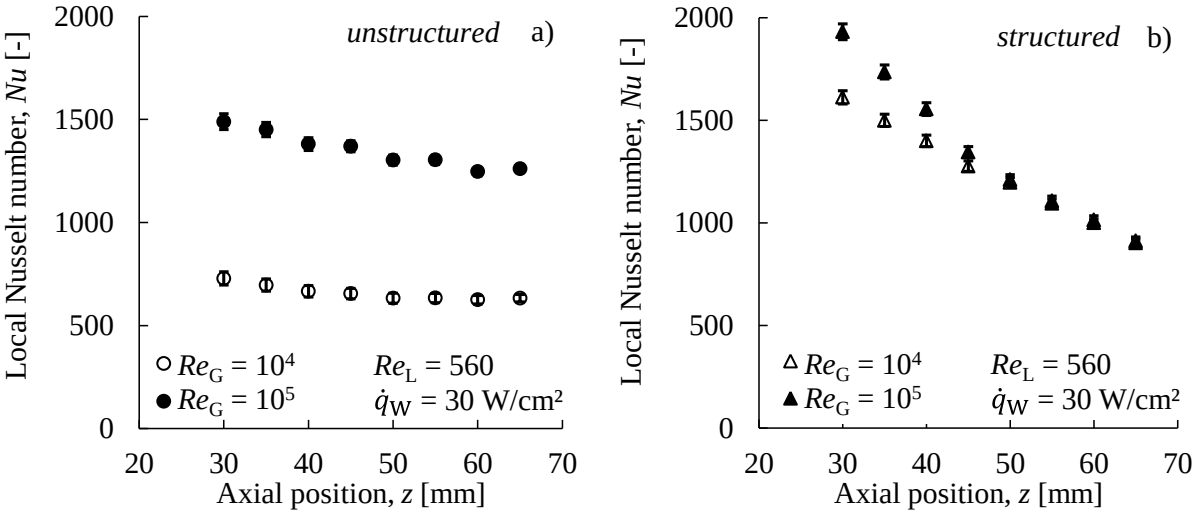

Figure 5. Local Nusselt number at $Re_L = 560$ and $q_W = 30$ W/cm² for a) unstructured and b) micro-structured surface.

The effect of gas Reynolds number on the behaviour of Nu is much weaker for micro-structured tube compared to that for an unstructured tube. A minor increase of the local Nusselt numbers can be seen for $Re_G = 10^5$ compared to the case $Re_G = 10^4$ within the range $z = 30$ mm to $z = 45$ mm. From $z = 50$ mm to $z = 65$ mm no significant change in the local cooling performance could be observed.

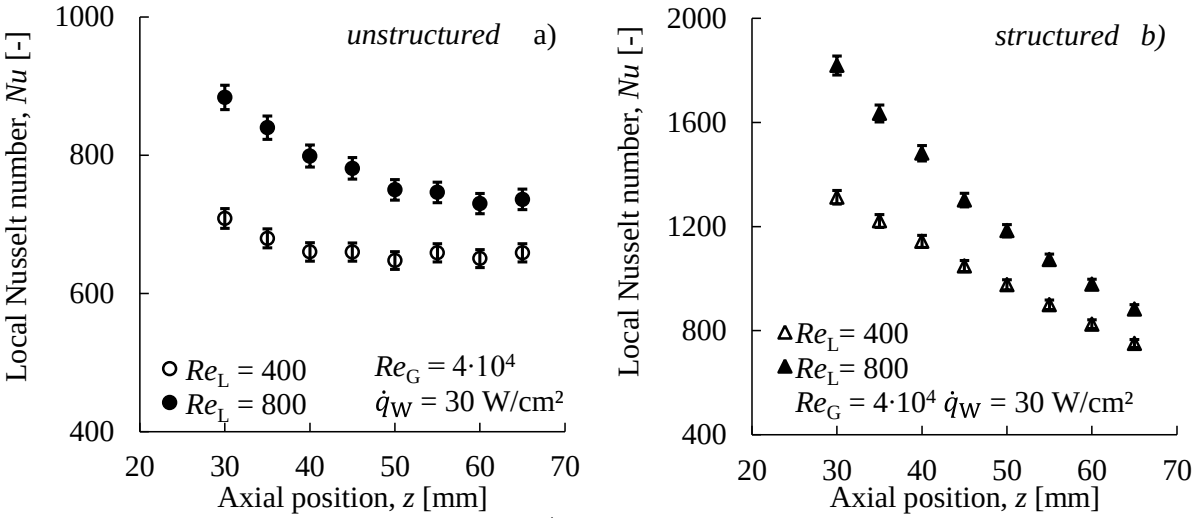

Figure 6. Local Nusselt number at $Re_G = 4 \cdot 10^4$ and $q_W = 30$ W/cm² for a) unstructured and b) micro-structured surface.

The effect of Re_L on the local Nusselt number distribution for the unstructured and micro-structured tubes is shown in Figure 6. A minor increase of Nusselt number with increasing of Re_L from 400 to 800 can be observed for both unstructured and micro-structured tubes. However, the local heat transfer coefficients in liquid film flow on the unstructured surface are less affected by Re_L than on the micro-structured surface one. Again, the local heat transfer coefficients on the micro-structured tube significantly exceed the heat transfer coefficients on the unstructured tube. The dependence of the mean Nusselt number on the gas and liquid Reynolds numbers for the unstructured and micro-structured tube is demonstrated in Figure 7. It is clearly seen that for nearly all combinations of experimental parameters the mean Nusselt number for the micro-structured tube exceeds the mean Nusselt number for the unstructured tube.

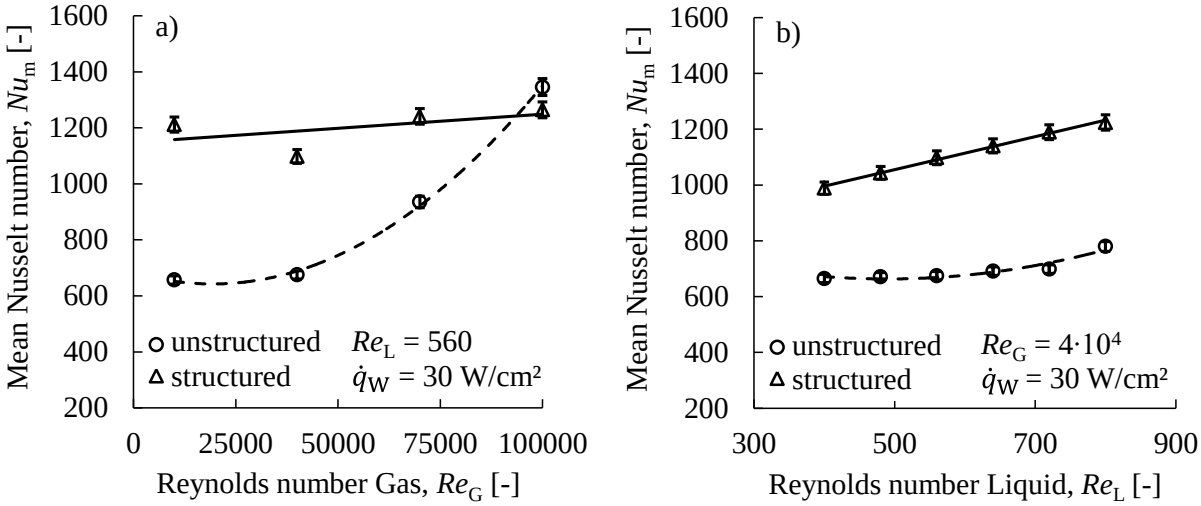

Figure 7. Development of the mean Nusselt numbers for unstructured and micro-structured surfaces at fixed q_W = 30 W/cm² for a) Re_L = 560 and varying Re_G, b) $Re_G = 4 \cdot 10^4$ and varying Re_L.

An enhancement of heat transfer coefficient of up to 80 % is achieved. It can be assumed that the structures on the surface have a significant disturbing effect and therefore cause strong instabilities in liquid film flow leading to an intensified mixing within the liquid layer [12, 13]. However, the increase in gas Reynolds number does not lead to a noticeable change of the heat transfer rate (Figure 7a). This can be attributed to the fact that the film flow has already reached a rather turbulent wavy state. A further increase of a shear stress at the liquid-gas interface by increasing the gas Reynolds number cannot generate an increase of mixing intensity. The heat transfer coefficient at the unstructured surface shows a stronger dependence on Re_G. By increasing the gas Reynolds number the mean Nusselt number significantly increases. This effect can be attributed to the increase of the film velocity with increasing of interfacial shear stress and to the intensification of the wavy motion. The difference in the mean Nusselt number decreases with increasing of the gas Reynolds number and eventually disappears at $Re_G = 1 \cdot 10^5$. Figure 7b illustrates the dependence of the mean Nusselt number on Re_L for the unstructured and the micro-structured tubes at $Re_G = 4 \cdot 10^4$ and a constant heat flux of 30 W/cm². The heat transfer coefficients on the micro-structured tube are higher than those on the unstructured surface, and the difference increases with increasing of Re_L. A significant linear growth of Nu_m with Re_L can be observed for the micro-structured tube. It can be assumed that the increase of Re_L leads to intensification of the motion in the vortices [12, 13] and to enhancement of the convective heat transfer. The heat transfer at the unstructured surface is weakly affected by Re_L. In this case, the liquid film flow increases its velocity by increasing Re_L, but the magnification is not sufficient to end up with a distinctive rise of the mean Nusselt number.

3.2. Local film break-up and rewetting

The film flow can exhibit topological changes. The local film rupture occurs preferentially at low flow rates and high wall heat fluxes. The dry patches can be rewetted by waves propagating along the flow direction. The film dry out and rewetting significantly affect the heat transfer. To study the influence of micro-structure on the film rupture and rewetting, the liquid film flow has been observed using the infrared thermography. Figure 8 shows the infrared images of the liquid-gas interface for the shear-driven liquid film flow along a micro-structured tube at $Re_L = 80$, $q_W = 30$ W/cm² and three distinct values of Re_G. The observation of local film break-up and rewetting on the micro-structured tube was not realizable for the previous ranges $Re_L = 400 – 800$ and varying Re_G. For this range the tubes surface was fully wetted and no break-up could be detected. However for $Re_L < 240$ and $Re_G = 7 \cdot 10^4$ and 10^5 the break-up of the film could be achieved. In the following paragraph selected infrared thermography records are shown exemplarily for $Re_L = 80$.

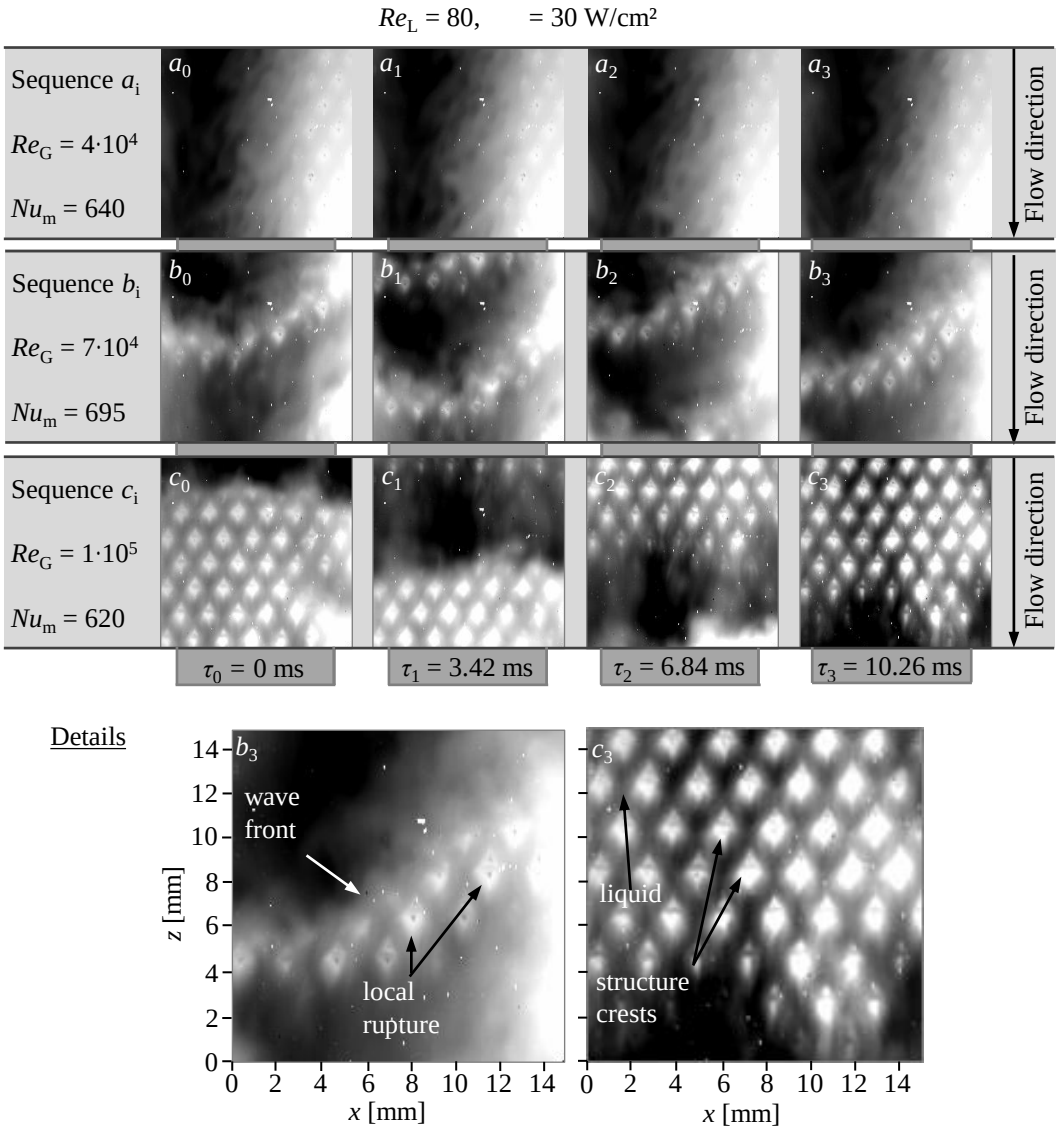

Figure 8. Film break-up and rewetting phenomena on micro-structured surface at fixed $Re_L = 80$ and $q_W = 30$ W/cm² and varying values for Re_G.

For each set of parameters, a sequence of four images corresponding to different time instants is represented (a_i, b_i, c_i). Light pixels correspond to high intensity of infrared radiation. In sequence a_i,

corresponding to $Re_G = 4 \cdot 10^4$, neither wave pattern nor film rupture can be seen. The film is flowing rather smooth. The film thickness over the pyramids is thinner than over the troughs of the wall structure, and therefore the temperature of the liquid-gas interface at the pyramids locations is higher. Increasing of gas Reynolds number leads to decrease of the average film thickness and to development of waves. At $Re_G = 7 \cdot 10^4$ (sequence b_i) a wave front propagating downstream can be observed. A region of thin film ahead of the wave crest can be seen as a thin light slightly curved horseshoe-shaped region. The position of pyramids under the thin film is easily recognizable due to additional local film thinning leading to high local interface temperatures and corresponding light color. In the detailed picture corresponding to image b_3 very small groups of dark pixels in the middle of regions corresponding to pyramids can be observed. These tiny dark regions may indicate that the crests of pyramids are dewetted. It can be assumed that the contrast in intensity between the light rhomb-shaped region and dark group of pixels in the middle of the region results from the difference in reflectivity between the water surface and the copper surface. At $Re_G = 10^5$ (sequence c_i), the average film thickness further decreases compared to the case $Re_G = 7 \cdot 10^4$. The waves are now elongated and its number per sequence is decreased. A large area of regular array of white rhombs appears in the field of view, whereas dark group of pixels indicating the dewetting of pyramid crests can be seen in the middle of many rhombs (Figure 8c_3). The next wave passing over the thin film area rewets the crests. It should be noted that the film flow with this combination of flow parameters cannot be realized on an unstructured tube due to the film instability and dry out over a large area. The comparison of the corresponding mean Nusselt numbers for each sequence shows that the convective heat transfer increases by the rise of Re_G from $4 \cdot 10^4$ to $7 \cdot 10^4$ due to higher interfacial shear forces leading to higher liquid velocities and intensification of the wavy motion. However, a further increase of Re_G up to 10^5 leads to a decrease of the mean Nusselt number. This decrease can be explained by the local dry out of the surface and the consequent decay of convective heat transfer.

4. Conclusions

This study presents the heat transfer measurements performed on shear-driven liquid films flowing on unstructured and micro-structured heated tubes. The local and mean Nusselt numbers have been determined in a wide range of liquid and gas Reynolds numbers. It has been found that the heat transfer coefficients on the micro-structured tube are higher than those on the unstructured tube. The differences between the heat transfer coefficients on the micro-structured and the unstructured tubes decreases with increasing gas Reynolds number but increases with the liquid Reynolds number. The Nusselt number on the micro-structured tubes depends on the liquid mass flow rate. The Nusselt numbers at the unstructured surface are dominated by the gas Reynolds number. The infrared thermography of the liquid-gas interface of a film flowing along a heated micro-structured tube has revealed a wavy film dynamics. A local dewetting of the pyramid crests and their rewetting by overflowing waves has been observed at elevated gas Reynolds numbers.

Acknowledgement

The authors acknowledge the financial support of the German Science Foundation (Deutsche Forschungsgemeinschaft) in the framework of the Collaborative Research Center 568, subproject A2.

Nomenclature

a, b, c	channel dimensions, [mm]	U_G, U_L	gas, liquid hydraulic diameter, [m]
d	tube diameter, [mm]	Re_G, Re_L	gas, liquid Reynolds number, [-]
h_Δ	height of pyramid, [µm]	$T_{G,in}, T_{L,in}$	gas, liquid inlet temperature, [°C]
H	passage height of gas stream, [mm]	$T_{W,i}$	local wall temperature, [°C]
I	electrical current, [A]	V	voltage, [V]
l_W	heated length of wall, [mm]	x, z	x-, z-axis, [mm]
M_G, M_L	gas, liquid mass flow rates, [kg·s^{-1}]	β_Δ	flank angle of pyramid, [°]
Nu	local Nusselt number, [-]	λ_L	liquid thermal conductivity, [W·m^{-1}·K^{-1}]

Nu_m	mean Nusselt number, [-]	μ_G, μ_L	gas, liquid dynamic viscosity, [Pa·s^{-1}]
q_W	wall heat flux, [W·m^{-2}]		

References

[1] Pommersberger K 2003 PhD Dissertation (German) TH Karlsruhe Institute ITS
[2] Arbeiter F 2002 Diploma Thesis (German) TH Karlsruhe Institute ITS
[3] Batarseh F Z, Roisman I V, Tropea C 2007 ASME Turbo Expo
[4] Schober P, Ebner J, Schäfer O, Wittig S 2003 Proc. 9th ICLASS
[5] Bar-Cohen A, Sherwood G, Hodes M, Solbreken G L 1995 IEEE Transactions on CPMT **18** 502-509
[6] Kabov O A , Zaitsev D V, Cheverda V V, Bar-Cohen A 2011 Exp. Therm Fluid Sci. **35** 825-831
[7] Fujita Y 1998 Heat Transfer Enhancement of Heat Exchangers, Ed. Kakaç S, Bergles A E, Mayinger F, Yuncu H, Kluwer Academic Publishers (Dordrecht, Netherlands) 325-346
[8] Gambaryan-Roisman T, Stephan P 2003 J. Enhanced Heat Transfer **10** 445-457
[9] Wierschem A, Aksel N 2004 Phys. Fluids **16** 4566-4574
[10] Helbig K, Nasarek R, Gambaryan-Roisman T, Stephan P 2009 J. Heat Transfer **131** 011601
[11] Stephan P, Busse C A 1992 Int. J. Heat Mass Transfer **35** 383-391
[12] Scholle M, Thompson H M, Aksel N, Gaskell P H 2007 Proc. Appl. Mech. **7** 3020003-3020004
[13] Scholle M, Haas A, Aksel N, Thompson H M, Hewson R W, Gaskell P H 2009 Int. J. Heat Fluid Flow **30** 175-185